Published online 22 November 2018

Nucleic Acids Research, 2019, Vol. 47, No. 1 ***93–102***
doi: 10.1093/nar/gky1189

Investigating the sequence-dependent mechanical properties of DNA nicks for applications in twisted DNA nanostructure design

Jae Young Lee[1], Young-Joo Kim[1], Chanseok Lee[1], Jae Gyung Lee[1], Hiromasa Yagyu[2], Osamu Tabata[3] and Do-Nyun Kim[1,4,*]

[1]Department of Mechanical and Aerospace Engineering, Seoul National University, Gwanak-ro 1, Gwanak-gu, Seoul 08826, Republic of Korea, [2]Department of Mechanical Engineering, Kanto Gakuin University, Yokohama 236-8501, Japan, [3]Department of Micro Engineering, Kyoto University, Kyoto Daigaku-Katsura, Kyoto 615-8540, Japan and [4]Institute of Advanced Machines and Design, Seoul National University, Gwanak-ro 1, Gwanak-gu, Seoul 08826, Republic of Korea

Received July 16, 2018; Revised November 06, 2018; Editorial Decision November 07, 2018; Accepted November 09, 2018

ABSTRACT

DNA nick can be used as a design motif in programming the shape and reconfigurable deformation of synthetic DNA nanostructures, but its mechanical properties have rarely been systematically characterized at the level of base sequences. Here, we investigated sequence-dependent mechanical properties of DNA nicks through molecular dynamics simulation for a comprehensive set of distinct DNA oligomers constructed using all possible base-pair steps with and without a nick. We found that torsional rigidity was reduced by 28–82% at the nick depending on its sequence and location although bending and stretching rigidities remained similar to those of regular base-pair steps. No significant effect of a nick on mechanically coupled deformation such as the twist-stretch coupling was observed. These results suggest that the primary structural role of nick is the relaxation of torsional constraint by backbones known to be responsible for relatively high torsional rigidity of DNA. Moreover, we experimentally demonstrated the usefulness of quantified nick properties in self-assembling DNA nanostructure design by constructing twisted DNA origami structures to show that sequence design of nicks successfully controls the twist angle of structures. Our study illustrates the importance as well as the opportunities of considering sequence-dependent properties in structural DNA nanotechnology.

INTRODUCTION

DNA nick or single-strand break, a common type of DNA damage, is the discontinuity in one of the sugar-phosphate backbones in the DNA double helix. DNA nicks inherently exist in most synthetic DNA nanostructures constructed by, for example, scaffolded DNA origami or single-stranded tile assembly methods, in which multiple oligonucleotides with programmed sequences are used (1–20). Due to its distinct mechanical behaviors, DNA nick can play a crucial role in determining the three-dimensional shape and structural properties of DNA nanostructures (7–14). For instance, nicks were deliberately used to design reconfigurable dynamic structures with the aid of a fuel strand (7,8) or create a sharp corner in the structure as they formed a kink when an internal force sufficiently high to break base-stacking interactions was applied (9). It was also reported that the design of nicks could affect the assembly yield and thermal stability of DNA nanostructures (10–12).

However, unlike regular DNA double helix whose mechanical properties and coupling effects (21,22) have been thoroughly characterized by both experiments (21–32) and molecular dynamics (MD) simulation (33–44), the mechanical properties of DNA nicks remain still elusive despite their importance. Only a few important characteristics of nicked base-pair (BP) steps were reported that nicked DNA behaved differently from regular DNA due to the relaxation of backbone constraint (45,46) while the base stacking interaction and hydrogen bonding could maintain the stability of nicked BP steps to some extent (46–48). A comprehensive study of mechanical properties of DNA nicks has not been reported yet, though their importance has increased since the sequence-level design of large DNA nanostructures becomes viable by introducing DNA strands with customized length and sequence (10,15).

*To whom correspondence should be addressed. Tel: +82 2 880 1647; Fax: +82 2 883 1513; Email: dnkim@snu.ac.kr

To extensively understand the mechanical characteristics of DNA nicks at single BP level and explore their utility in DNA nanostructure design, we first investigated the sequence-dependent mechanical properties of BP steps with a particular focus on the effect of nicks by performing MD simulation for a complete set of distinct double-stranded DNA oligomers constructed using all possible BP steps (ten without a nick and sixteen with a nick). Six primary mechanical rigidities and fifteen coupling coefficients were quantified extensively for all BP steps from MD trajectories, revealing the significant and highly sequence-dependent reduction (28–82%) of the torsional rigidity by nicks. Then, we applied the identified mechanical properties of BP steps to DNA origami design and demonstrated for the first time that the global twist angle of the bundle structure could be modulated by designing the sequence of nicked BP steps therein from atomic force microscopy (AFM) analysis. Since it is easy to program the sequences at nick sites in the design of self-assembling DNA nanostructures, we expect that our mechanical data and sequence-design approach for precise control would be useful in the field of structural DNA nanotechnology.

MATERIALS AND METHODS

Generation of DNA oligomers

There exist ten distinct regular BP steps without a nick: AA/TT, AG/CT, GA/TC, GG/CC, AC/GT, AT/AT, GC/GC, TG/CA, TA/TA, and CG/CG steps. We used these regular BP steps to build ten 42-BP-long DNA double helices, each of which makes four complete turns about its helical axis. We chose this duplex length to prevent the behavior of the central BP step from being significantly affected by the highly flexible and localized motion of duplex ends (38,39). A freely available program 3DNA was used for the construction of DNA oligomers with the default geometry of generic B-form DNA (49). To investigate the effects of nicks, we constructed nicked DNA double helices as well by introducing a single-strand break in the middle of each BP step resulting in structures with sixteen unique nicked BP steps: AA/TnT, AG/CnT, GA/TnC, GG/CnC, AnA/TT, AnG/CT, GnA/TC, GnG/CC, AC/GnT, AnC/GT, AT/AnT, GC/GnC, TG/CnA, TnG/CA, TA/TnA, and CG/CnG steps (Supplementary Table S1). The phosphorus atom and the attached oxygen atoms of the backbone at the nick site between the bases P and Q were removed in nicked BP steps (46,48). Here, we represented a regular BP step as MN/PQ where M, N, P, and Q denote one of the canonical nucleobases (A, G, T, and C) and a nicked BP step as MN/PnQ or MnN/PQ where a nick existing between bases was indicated by 'n' (Figure 1A).

MD simulation of DNA oligomers

We performed MD simulations to investigate the conformational dynamics of the DNA double helices using a freely available program, NAMD (50) with the CHARMM36 force field (51) for nucleic acids. The CHARMM36 force field was adopted since it showed general agreements with experiments from the previous MD studies of DNA nanostructures (4–6,16,17). Each DNA oligomer was explicitly solvated in a 60 Å × 60 Å × 180 Å cubic TIP3P water box (52). In this study, since the mechanical properties of nicked BP steps were expected to mainly contribute to the analysis and design of structural DNA nanotechnology where 10–20 mM $MgCl_2$ condition have generally been selected, MD simulation was performed under a $MgCl_2$ condition of 10 mM. The distance between the DNA oligomer and the cell boundary was approximately 20 Å, and periodic boundary conditions were applied. The short-range electrostatic and van der Walls potentials were smoothly reduced with the switching scheme active above 12 Å cut-off. We employed the Particle Mesh Ewald (PME) method (53) with a grid spacing of 1.0 Å to consider long-range electrostatic interactions efficiently. The static energy of each system was minimized for 20 000 steps using the conjugate gradient algorithm. Trajectories of 100 ns were obtained under the isobaric-isothermal (NPT) ensemble after a pre-equilibrium process of 10 ns. We maintained the pressure at one bar using the Nosé–Hoover Langevin piston scheme (54) and the temperature at 298 K with Langevin thermostat (50) with a damping constant of 0.1 ps^{-1}. The equilibrated root-mean-square deviation (RMSD) values of DNA oligomers were obtained from their minimized coordinates during MD simulation (Supplementary Figure S1).

Mechanical rigidities and coupling coefficients

We analyzed and compared the conformational dynamics of regular and nicked BP steps using the obtained 100-ns-long MD trajectories for each of these twenty-six DNA oligomers in equilibrium. To measure the mechanical properties at BP level from MD trajectories, we employed six BP step parameters following the definition in 3DNA (49) and quantified the relative motion of two adjacent BPs in regular and nicked BP steps (Figure 1B, Supplementary Figures S2, and S3). The BP step parameters consist of three rotational and three translational rigid-body degrees of freedom defined as tilt (τ), roll (ρ), twist (ω), shift (Dx), slide (Dy), and rise (Dz), describing the stacked configuration of one BP relative to its neighbor (Supplementary Tables S2 and S3). Here, it was confirmed that the BP step parameters estimated from the MD trajectories were statistically different at the significance level of 0.01 according to the t-test comparing the regular and corresponding nicked BP steps. The mechanical rigidities (B_τ, B_ρ, C, Y_{Dx}, Y_{Dy}, and S) and coupling coefficients (g_{ij}) of regular and nicked BP steps were then estimated using the covariance matrix (36,37,43,55) (Figure 1C and Supplementary Tables S4-S7). The stiffness matrix was calculated from the covariance matrix of the BP step parameters based on quasi-harmonic approximation as $\mathbf{K} = k_B T \mathbf{F}^{-1}$ where $\mathbf{K}$ and $\mathbf{F}$ are the stiffness matrix and the covariance matrix, k_B is the Boltzmann constant, and T is the absolute temperature, respectively (Supplementary Methods S1 and S2). We confirmed that highly flexible motion of duplex ends did not affect the behavior of the central BP step since sequence-dependent mechanical rigidities were observed with the repeated pattern of sequence variation except for terminal BP steps (Supplementary Figure S4). Additional MD simula-

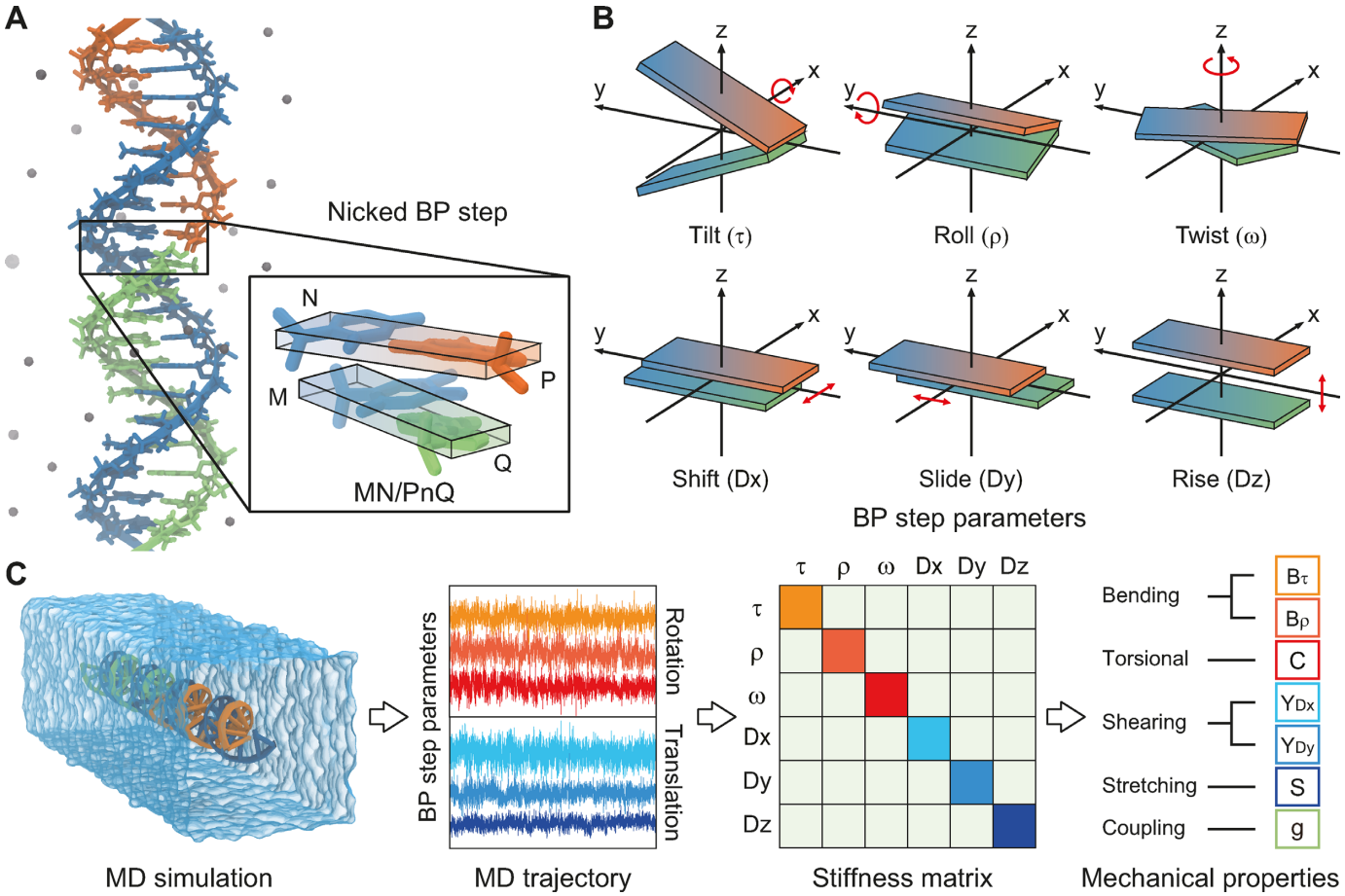

Figure 1. Schematic illustration of investigating the mechanical properties of nicked base-pair (BP) step. (**A**) A nicked BP step in a DNA double helix. Blue strand is well-connected, whereas the backbone is broken between the orange and green strands indicating a nick. The enlarged figure shows a nicked MN/PnQ step where M, N, P, and Q represent one of the canonical nucleobases (A, G, T, and C), and the nick exists between P and Q bases indicated by 'n'. The nicked BP step is illustrated with two successive BPs represented by thin and long plates. (**B**) Six BP step parameters. These BP step parameters were defined in 3DNA (49) and were determined as the relative rigid-body modes of the two BPs. The rigid-body rotations of a BP step were denoted by tilt (τ), roll (ρ) and twist (ω), and similarly, the rigid-body translations were denoted by shift (Dx), slide (Dy) and rise (Dz) for the *x*, *y*, and *z*-axes, respectively. (**C**) Derivation of mechanical properties. Mechanical rigidities and coupling coefficients were obtained from the MD trajectory of BP step parameters.

tions were performed to investigate the effects of the different parmbsc1 force field (56), ion conditions and neighboring sequences of BP steps (Supplementary Note S1, Supplementary Figures S5–S8, and Supplementary Tables S8–S13).

Design and simulation of twisted DNA origami structures

To identify and apply mechanical properties of BP steps to DNA nanostructure, we designed six-helix-bundle (6HB) DNA origami structures with BP-insertion. Our theoretical analysis suggested that the ratio of torsional rigidity (C) to bending rigidity (B) of DNA helix dominates the twist angle of bundle structure for the given number of inserted BPs (Supplementary Note S2). The single equivalent bending rigidity (B) was determined by the harmonic mean of anisotropic tilt and roll bending rigidities (B_τ and B_ρ) (Supplementary Method S3). Here, we defined C/B ratio of nicked BP steps normalized by corresponding regular BP steps as C/B ratio $= \frac{(C/B)^{nicked}}{(C/B)^{regular}}$. The standard deviations of $(C/B)^{regular}$, $(C/B)^{nicked}$, and C/B ratios were calculated as $\sigma_{\alpha/\beta} = \frac{\alpha}{\beta}\sqrt{\frac{\sigma_\alpha^2}{\alpha^2} + \frac{\sigma_\beta^2}{\beta^2}}$, where α and β represent the mean values of two different properties, and σ_α and σ_β indicate the standard deviations (Supplementary Table S14). This sequence-dependent C/B ratio quantified the potential effect of a nick on the twist angle with respect to an ideal 6HB structure consisting of regular BP steps only. We also observed that a similar trend of C/B ratio was obtained with the parmbsc1 force field (56) (Supplementary Note S1 and Supplementary Figure S8). Based on C/B ratio data from MD simulation, we controlled the global twist angle of 6HB structures by deliberately locating the sequence of nicked BP steps where staple strands met (Supplementary Tables S15–S17). To approximately predict the twist angle of the 6HB structures, the elastic network-guided MD simulation (5) was performed on the segments of the 6HB structures (Supplementary Figure S9, Supplementary Methods S4, and S5). We also conducted the CanDo simulation (9,17) of entire 6HB structures to observe the change in twist angle of the structures with different mechanical

rigidities of nicks (Supplementary Method S6 and Supplementary Figure S10).

Preparation of DNA origami structures

Sequence and connectivity information in 6HB DNA origami structures were designed using caDNAno software (57), and the sequences of all constituting staples were listed in Supplementary Table S18. We purchased the M13mp18 single-stranded DNA of 7249 nucleotides for scaffold strands from New England Biolabs (N4040s), staple strands less than 50 nucleotides from Bioneer Corporation, and reagents from Sigma-Aldrich. All oligonucleotides were purified by the reverse-phase cartridge (Bio-RP) method provided by Bioneer Corporation. We also used the staples purified with the polyacrylamide gel electrophoresis (PAGE) method to examine any potential effect of purification method, but no clear dependence of the results on the purification method was observed (Supplementary Note S3, Supplementary Figures S11, S12, and Supplementary Table S19). For the assembly of DNA structures, the folding mixture containing 10 nM of scaffold DNA, 100 nM of each staple strand, 20 mM of $MgCl_2$, and 1 × TAE buffer (40 mM Tris-acetate and 1 mM EDTA) was annealed using a thermocycler (T100, Bio-Rad) with a temperature gradient from 80 to 65°C by −0.25°C per minute and 65–25°C by −1°C/h.

AFM analysis

To observe the shape of the assembled 6HB DNA origami structures, we diluted the samples to approximately 0.5 nM with a folding buffer of 1× TAE and 20 mM $MgCl_2$, and the samples were deposited on a freshly cleaved mica substrate (highest grade V1 Mica, Ted-Pella Corporation). After incubation for 5 minutes, the substrate was washed with DI water and gently dried by N_2 gun (<0.1 kgf cm^{-2}). AFM images were taken by NX10 (Park Systems) using non-contact mode in SmartScan software. A PPP-NCHR probe with a spring constant of 42 N m^{-1} was used in the measurements (Nanosensors). Measured images were flattened with linear and quadratic order using XEI 4.1.0 program (Park Systems). For all experimental cases, at least eleven positions on the mica substrate were scanned and more than thousand monomer structures were collected (Supplementary Figure S12 and Supplementary Tables S16–S18). Here, the twist angle of structures was indirectly measured from two-dimensional AFM images. Each monomer structure took either the cis state (flags in the same side) or the trans state (flags in the opposite sides) in the AFM image. The number of monomeric structures in each state was then counted to calculate the trans ratio as the number of monomeric structures in the trans state divided by the total number of monomers. The trans ratio (TR) was finally converted to the twist angle from the theoretical function (3) as $TR = f(\Phi_0, \sigma, k)$, where Φ_0 is the equilibrium twist angle of structures, σ is the standard deviation of the twist angle by thermal fluctuation estimated as 0.7524 rad for the torsional persistence length of 530 nm proposed in the previous studies (3,18) and the axial length of 300 nm in our 6HB structures, and k is a parametric integer indicating the range of twist angle of 6HB structures (Supplementary Method S7). We calculated the trans ratios for each AFM image of a structure from which their mean and standard deviation were calculated.

Agarose gel electrophoresis

Assembled 6HB DNA origami structures were electrophoresed using 1.5% agarose gels containing 0.5× TBE (45 mM Tris-borate and 1 mM EDTA), 12 mM of $MgCl_2$ and 0.5 μg ml^{-1} of ethidium bromide (EtBr, Noble Bioscience Corporation). The 6HB structures were then electrophoresed for 1.5 h at 75 V bias voltage (∼3.7 V cm^{-1}) in an ice-water cooling chamber (i-Myrun, Cosmo Bio Corporation). Gel imaging was performed using a Gel-Doc XR+ device and Image Lab v5.1 program of Bio-Rad (Supplementary Figure S13).

RESULTS

Mechanical rigidities

We first examined the mechanical rigidities of regular BP steps (Figure 2). On the whole, the mechanical rigidities of regular BP steps were consistent with the ones determined in other experimental or computational studies. The calculated bending, torsional, shearing, and stretching rigidities were $B_\tau^{regular} = 246 \pm 56$ pN nm^2, $B_\rho^{regular} = 158 \pm 24$ pN nm^2, $C^{regular} = 314 \pm 43$ pN nm^2, $Y_{Dx}^{regular} = 418 \pm 100$ pN, $Y_{Dy}^{regular} = 738 \pm 267$ pN, and $S^{regular} = 1825 \pm 377$ pN, respectively (Supplementary Table S4), which were comparable to the reference values in literature (21–32,37–42) ($B_\tau^{ref} = 236 \pm 27$ pN nm^2, $B_\rho^{ref} = 133 \pm 34$ pN nm^2, $C^{ref} = 317 \pm 108$ pN nm^2, $Y_{Dx}^{ref} = 323 \pm 68$ pN, $Y_{Dy}^{ref} = 526 \pm 155$ pN, and $S^{ref} = 1343 \pm 631$ pN). Here, B_τ and B_ρ represent the bending rigidities corresponding to tilt and roll, C is the torsional rigidity, Y_{Dx} and Y_{Dy} denote the shearing rigidities in shift and slide, and S is the stretching rigidity. Our results confirmed the known fact that BP steps are more flexible to bend or shear toward the grooves than toward phosphate backbones because atoms are distributed wider in the direction of backbone sites, and more severe steric clashes occur when tilted or shifted than rolled or slid, respectively (33).

The obtained mechanical rigidities clearly show, as in the previous studies (38–41), the dependence on the sequence of a BP step including the effect of stacking order due to the chirality of DNA. For example, GC/GC and CG/CG steps exhibited the highest and lowest bending rigidities in roll, respectively, among all regular BP steps even though their constituent nucleobases were the same. A similar difference in the mechanical rigidities was observed for AT/AT and TA/TA steps as well. Further investigation of the results confirmed the dependence of DNA rigidities on the BP step group (Figure 2). The regular BP steps can be categorized into three BP step groups: purine-purine group denoted here as RR/YY (AA/TT, AG/CT, GA/TC, and GG/CC steps), purine-pyrimidine group as RY/RY (AC/GT, AT/AT, and GC/GC steps), and pyrimidine-purine group as YR/YR (TG/CA, TA/TA, and

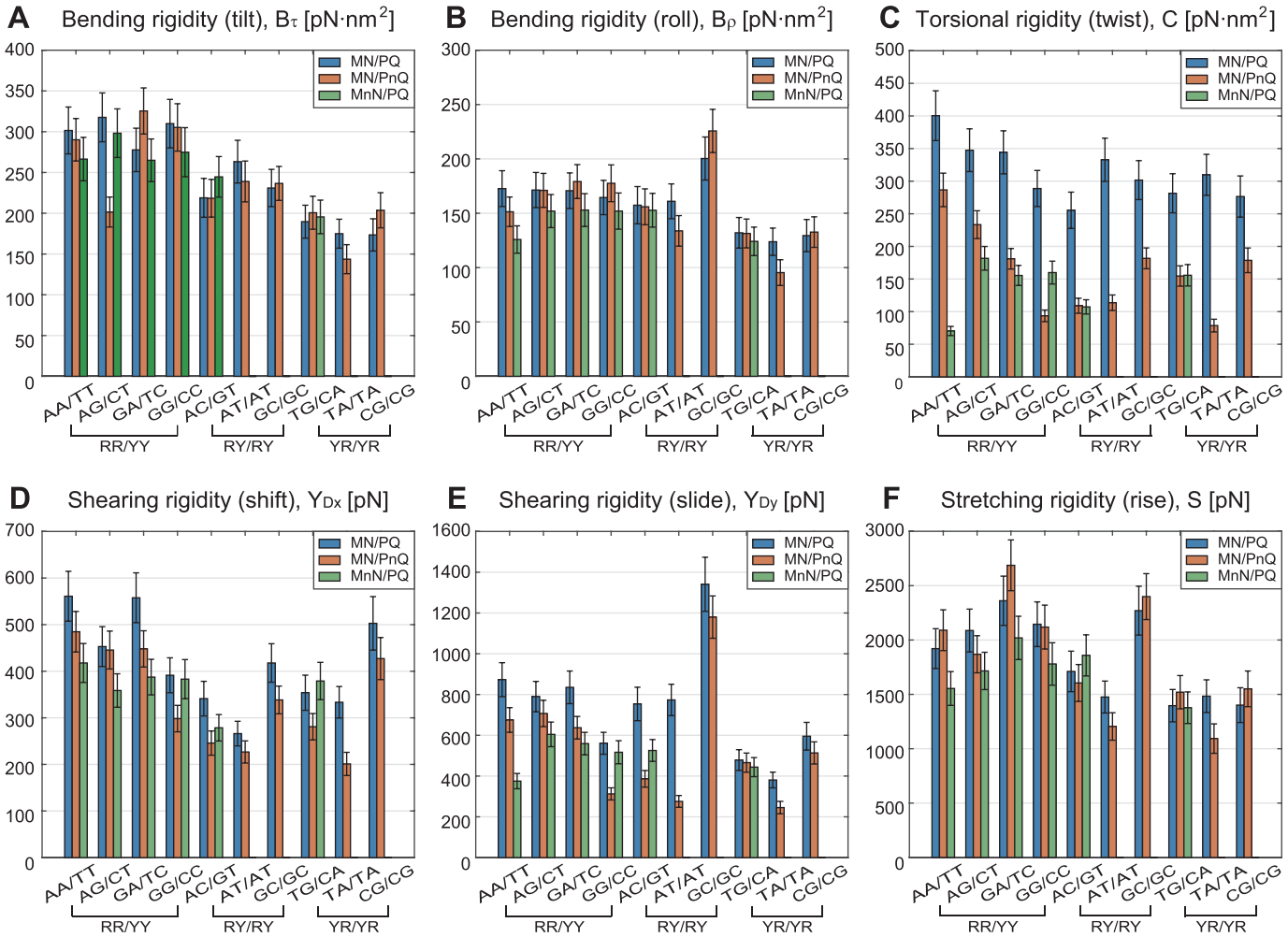

Figure 2. Mechanical rigidities of regular and nicked BP steps. Six figures represent (**A**) tilt-bending, (**B**) roll-bending, (**C**) torsional, (**D**) shift-shearing, (**E**) slide-shearing, and (**F**) stretching rigidities, respectively using average mechanical rigidities (Supplementary Tables S4 and S5). Blue represents the rigidities of regular BP steps (MN/PQ) while orange and green indicate the values of nicked BP steps (MN/PnQ or MnN/PQ). The standard deviation of each rigidity was estimated by multiplying the stiffness values of BP steps with the standard deviation of the rise.

CG/CG steps) where R and Y represent purine and pyrimidine, respectively. RR/YY group demonstrated relatively high rigidities, in general, whereas YR/YR group exhibited low rigidities for all deformation modes. RY/RY group had intermediate rigidities, but GC/GC step was exceptionally stiffer in deformation modes of roll, slide, and rise than the other BP steps. It was reported that the structural difference among these BP step groups determined the stereochemical characteristics of a BP step affecting the BP step parameters and mechanical rigidities in equilibrium (33,35). Also, these results were qualitatively parallel to those of earlier computational studies demonstrating that, for dinucleoside monophosphates, RR pair showed the strongest stacking force followed by RY pair while YR and YY pairs had relatively weaker stacking force similar to each other (58,59).

When introducing a nick to each regular BP step, we observed a considerable decrease in the torsional rigidity from $C^{regular} = 314 \pm 43$ pN nm^2 to $C^{nicked} = 153 \pm 57$ pN nm^2 on average amount approximately to 52% reduction (Figure 2C, Supplementary Tables S4, and S5). Softening effect of a nick in torsion was universal regardless of the location of the nick (MnN/PQ or MN/PnQ steps) as well as the sequence variation. Strikingly, we observed a drastic effect of nick location on the torsional rigidity for AA/TT step. The maximum and minimum reductions were 82% of AnA/TT step and 28% of AA/TnT step, respectively. AA/TT step showed the highest torsional rigidity among all regular BP steps, and it was still the strongest in torsion when a nick was introduced at the TT site (AA/TnT step). However, when a nick was located at the AA site (AnA/TT step), the torsional rigidity was significantly reduced and became the most flexible nicked BP step. For the shearing rigidities, smaller softening effect of a nick was predicted where the reduction ratio ranged from 2% (AG/CnT step) to 40% (TA/TnA step) for shift, and from 3% (TG/CnA step) to 64% (AT/AnT step) for slide leading to the mean reduction ratio of 22% (Figure 2D and E). Except for the case of TnG/CA whose shearing rigidity in shift was slightly increased by 7%, all the other BP steps became flexible in both shift and slide with a nick. These results suggest that one

of the primary structural roles of a nick could be the relaxation of torsional constraint by sugar-phosphate backbones known to be responsible for relatively high torsional rigidity of DNA (60–62).

On the contrary, the bending and stretching rigidities of nicked BP steps (B_{τ}^{nicked} = 244 ± 49 pN nm^2, B_{ρ}^{nicked} = 151 ± 29 pN nm^2, and S^{nicked} = 1778 ± 421 pN) did not considerably deviate from the rigidities of regular BP steps on average with the maximum deviations of 22% for bending (AnA/TT step) and 26% for stretching (TA/TnA step), respectively (Figure 2A, B, and F). More interestingly, we could observe not only softening but also stiffening effect of a nick depending on the sequence of BP steps. Six nicked BP steps (GA/TnC, AnC/GT, GC/GnC, TG/CnA, TnG/CA, and CG/CnG) showed the increased bending rigidity in tilt by 10% on average, four BP steps (GA/TnC, GG/CnC, GC/GnC, and CG/CnG) for the bending rigidity in roll by 7%, and six BP steps (AA/TnT, GA/TnC, AnC/GT, GC/GnC, TG/CnA, and CG/CnG) for the stretching rigidity by 9%. These results suggest that BP steps may adopt another equilibrium configuration where the base stacking force, a dominant factor to maintain the stability of BP steps without covalent bonds (46–48), becomes stronger. Perhaps, this stable equilibrium configuration is inaccessible for regular BP steps due to the constraints by backbones but becomes accessible for certain BP steps when one of the backbones was broken, and the backbone restrictions were released in consequence. To identify the stiffened conformation from MD traces, we looked more closely into GA/TnC, GC/GnC, and CG/CnG steps whose stretching and bending rigidities were increased by a nick. We found that these steps commonly exhibited the decrease in roll and shift parameters (Supplementary Figures S2 and S3), indicating that BP steps bend toward the minor groove. This result agrees with a previous study where the persistence length of DNA was found to be larger when BP steps bent toward the minor groove than when toward the major groove due to the difference in groove hydration (44).

We observed that a nick did not change the overall dependence of DNA rigidities on the BP step group. However, the location of a nick was a crucial factor in determining the mechanical rigidities of the purine-purine group (RR/YY). RR/YnY group was usually stiffer than RnR/YY group in every deformation mode and, on certain occasions, even stiffer than regular RR/YY group. This was probably because RR pair exhibited much stronger stacking forces than YY pair and, therefore, dominated the mechanical rigidities of regular and nicked RR/YY group. As a result, RR/YnY group were naturally stiffer than RnR/YY group in general and could be even stiffer than regular RR/YY group in some instances if a nick induced a conformational transition of BP step to a more stable configuration.

Mechanical coupling coefficients

The stiffness matrices obtained from MD trajectories of all regular and nicked BP steps also provide the mechanical coupling coefficients (g_{ij}), which are the off-diagonal terms of the stiffness matrix multiplied by the mean rise, indicating the correlation between two BP step parameters. Results indicated that nicks weakened, to some extent, the overall mechanical coupling of BP step parameters, but their effect was not strong enough to alter overall pattern of the stiffness matrix or the correlation map (Figure 3, Supplementary Tables S6, and S7). Positively correlated BP step parameters in a regular BP step remained positively correlated in the corresponding nicked BP step as well. Similarly, highly correlated ones remained highly correlated with a nick. We could reproduce one of the well-known mechanical couplings, the twist-stretch coupling, which is the counterintuitive mechanical behavior of DNA revealed by recent experimental (21,22) and computational studies (37,42,43). Negative mechanical coupling coefficient of twist and rise, which we obtained as $g_{\omega Dz}^{regular}$ = –277 ± 60 pN nm, was consistent with the reference value, $g_{\omega Dz}^{ref}$ = –222 ± 12 pN nm, reported in previous MD study (42), which was predicted to reduce to $g_{\omega Dz}^{nicked}$ = –178 ± 61 pN nm for nicked BP steps on average in this study. We also obtained negative mechanical coupling coefficients for twist-slide as $g_{\omega Dy}^{regular}$ = –149 ± 57 pN nm and $g_{\omega Dy}^{nicked}$ = –101 ± 50 pN nm, respectively, in agreement with the reported value of $g_{\omega Dy}^{ref}$ = –207 ± 95 pN nm (37) demonstrating that, when DNA is over-twisted, it elongated with the reduction of the inter-strand distance corresponding to slide in our study as long as base-stacking and base-pairing were maintained without base separation.

Sequence design of nicks for twist control of DNA origami structures

Our comprehensive and quantitative investigation on DNA nicks revealed that the major mechanical role of nicks in the stacked configuration is the sequence-dependent reduction of torsional rigidity. This torsion-softening effect of nicks is applicable particularly to twisted DNA origami bundle structures as multiple nicks scattered all over the section, and their locations can be easily adjusted. In order to experimentally demonstrate the usefulness of mechanical rigidities quantified for all regular and nicked BP steps in designing synthetic DNA nanostructure, we designed 6HB DNA origami structures whose ten twisting blocks controlled global twist angle in the middle of the structure (Figure 4A). In a twisting block, each helix was 42-BP-long, the number of inserted BPs was fixed, and six locations of nicks was selected by adjusting the length of the constituent staple strands (Figure 4B). Inserted BPs to twisting blocks introduce the torsional mismatch of cross-linked DNA helices (2), consequently inducing the torsional strain energy by the geometric constraints. We modulated the twist deformation from induced torsional energy in twisting blocks by controlling the rigidities of nicks through sequence design based on our rigidity data, thereby regulating globally twisted shape of the 6HB structure. We expected that only the twist angle of structures could be controlled by nicks inferred from a previous study that revealed almost no effect of nicks on the bending rigidity of DNA nanotubes (19). Here, we might need to take the change in the equilibrium twist parameter by a nick into consideration. In the 6HB twisting block design with 2-BP-insertion, four BPs were totally inserted into each helix in order to increase the twist angle as a multiple of intrinsic helical rotation (Supplementary Figure S9), which is ∼138° assuming the mean twist parameter of 34.51° for

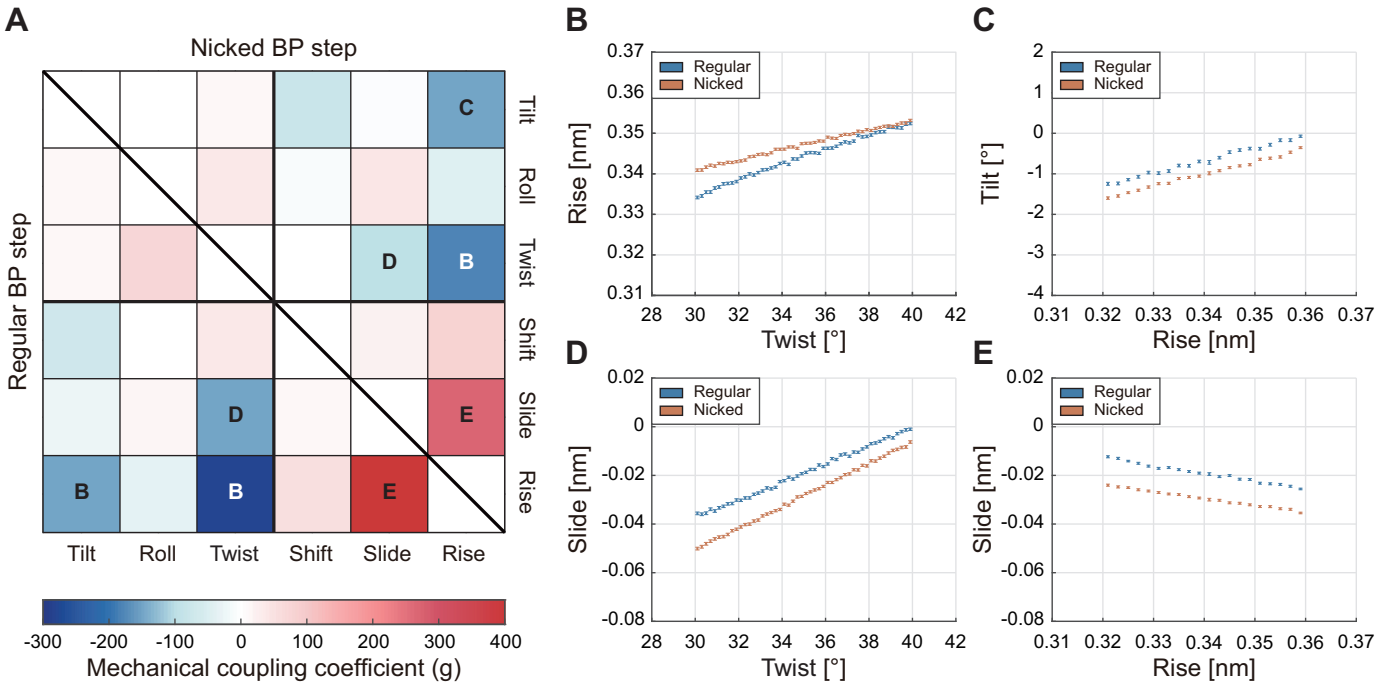

Figure 3. Mechanical coupling of regular and nicked BP steps. (**A**) Pixel plot of mechanical coupling coefficients. Overall mechanical coupling coefficients in off-diagonal squares are illustrated with blue and red color gradient. Diagonal values for rigidities are not illustrated. Lower left and upper right squares divided by a slope represent coupling coefficients of regular and nicked BP steps, respectively. Four three by three plots also subdivide this pixel plot with different coupled modes: the upper left plots for rotation-rotation [pN nm^2], the upper right and lower left plots for rotation-translation [pN nm], and the lower right plots for translation-translation [pN]. (**B–E**) Correlation plots of four primary mechanical coupling coefficients. These plots represent the correlation between (**B**) rise to twist, (**C**) tilt to rise, (**D**) slide to twist, and (**E**) slide to rise. Domains were divided into intervals of 0.2° and 0.002 nm for twist and rise where error bars were obtained as standard errors of the mean.

regular BP steps (Supplementary Table S2). However, only one nicked BP step exists in each helix whose highest change in the twist parameter is about 6° for AnC/GT step. This suggests that the twist change by a nick for a helix would be only 4% of that by BP-insertions at most (Supplementary Tables S2 and S3). Hence, we concluded that the change in the equilibrium twist at a nick site can be ignored.

According to our theoretical analysis, the C/B ratio dominates the twist angle of bundle structure with BP-insertion (Supplementary Note S2). The C/B ratio is also certainly sequence-dependent and always smaller than one since the nick reduces the torsional rigidity while the bending rigidity does not considerably change. The C/B ratios for all nicked BP steps determined from our MD results range from 0.23 (AnA/TT step) to 0.81 (AG/CnT step) with the following order: AG/CnT > AA/TnT > GnG/CC > CG/CnG > AnG/CT > TnG/CA > GC/GnC > TG/CnA > GnA/TC > GA/TnC > AC/GnT > AnC/GT > AT/AnT > TA/TnA > GG/CnC > AnA/TT (Figure 4D and Supplementary Table S14). Utilizing the C/B ratio data, we designed two pairs of stiff, moderate, and flexible structures with 2-BP-insertion by choosing the location of the nicks to control the C/B ratio. The stiff and flexible structures were designed by choosing nick sequences among the nine possible locations to maximize and minimize the C/B ratio, respectively (Figure 4C). The location of nicks was adjusted to create two similar pairs of stiff and flexible structures, suggesting that the mean C/B ratios accounting for sixty nicked BP steps in ten twisting blocks ranged from 0.302 for the flexible design to 0.674 for the stiff design (Supplementary Table S15). Two moderate structures were designed to have the middle C/B ratio of approximately 0.488 which is in the mean of C/B ratios used for stiff and flexible designs. The stiff design with the higher C/B ratio was expected to result in a larger twist angle than the flexible design since higher torsional strain energy was induced under the same torsional mismatch due to inserted BPs (Figure 4E), which was confirmed by CanDo simulation (Supplementary Figure S10).

The twist angle of self-assembled 6HB structures was characterized by AFM analysis. The results of agarose gel electrophoresis and AFM images indicated that monomeric structures were appropriately folded and the variations in nick position hardly affected the folding yield (Supplementary Figures S12 and S13). The structures took either the trans state (flags in the opposite sides) or the cis state (flags in the same side) in the AFM image (Figure 4F and Supplementary Figure S12). The number of monomeric structures in each state was reduced to the trans ratio and twist angle (Figure 4G and Supplementary Table S16). Based on the MD results for a twisting block with 2-BP-insertion suggesting that the entire structures would be twisted by 550 ± 12° (Supplementary Figure S9), the twist angles converted from the trans ratio were estimated as 614–624° for the stiff designs, 602–612° for the moderate designs, and 582–585° for the flexible designs on average. These experimental results confirmed our expectation based on theoretical analysis that the stiff design could be more twisted than the flexi-

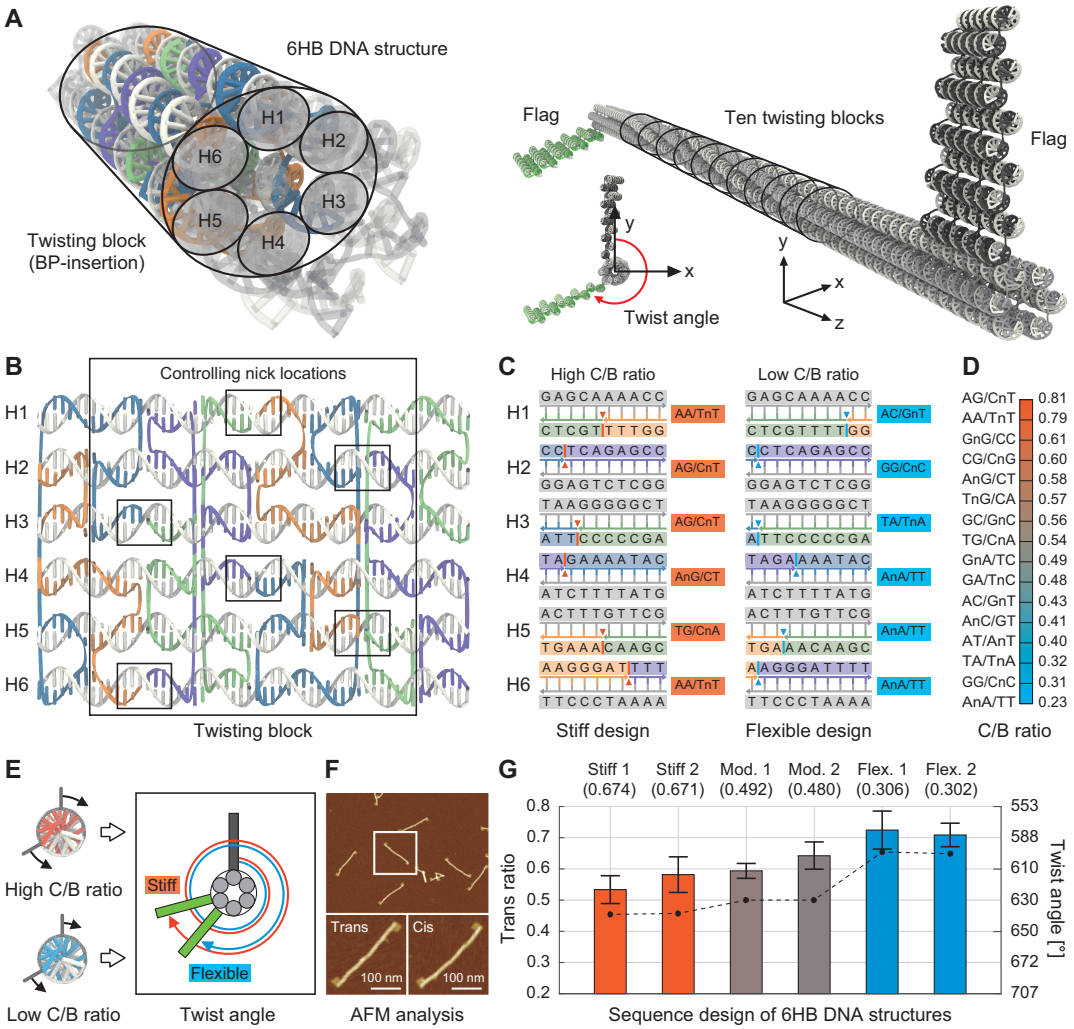

Figure 4. Sequence design to control the twist of DNA origami structures. (**A**) Schematic illustration of a 6HB DNA origami structure. 6HB structures were designed to include ten twisting blocks composed of H1-H6 helices with BP-insertion. Two terminal flags showed the torsional deformation. (**B**) The development figure of a twisting block. 2-BPs were inserted into all 14-BP-long strands resulting in 16-BP-long strands. Any BP was not inserted into the other strands. In six regions where nicks exist, the locations of the nicks were programmed to control the sequence-dependent rigidities with at least 4-BPs away from Holliday-junctions. (**C**) An example design of a twisting block to design stiff and flexible structures. White and colored strands represent scaffold and staple strands, respectively. The nicks were selected to induce the highest and lowest C/B ratio among possible nine positions of staple strands. (**D**) List of C/B ratio. C/B ratio of nicked BP steps was defined as the ratio of torsional rigidity to bending rigidity normalized by corresponding regular BP steps. The standard deviations of C/B ratio were listed in Supplementary Table S14. (**E**) Mechanical analysis of bundle DNA structures with BP-insertion. The twist angle of the structure is induced by the torsional strain energy due to the inserted BPs and controlled by C/B ratio. (Supplementary Note S2). (**F**) AFM analysis of trans and cis monomers (Supplementary Figure S12). (**G**) Results of trans ratio and twist angle from sequence design of nicks. Two pairs of stiff, moderate, and flexible structures are represented as descending order of mean C/B ratio in brackets. The trans ratio was calculated as dividing the number of trans monomers by the total number of monomers. The standard deviation of trans ratio was calculated using the trans ratios of AFM images (Supplementary Tables S16 and S17). The twist angle predicted by CanDo simulation is illustrated as the dotted line (Supplementary Figure S10).

ble design. Considering the wide controllable range of C/B ratio, even finer control on the twist angle were also available by using various sets of nicked BP steps for the same structure. In addition, we performed the t-test for the trans ratio to check the statistical significance of the difference in the twist angle. It confirmed that the trans ratios of 2-BP-inserted structures were statistically different at the significance level of 0.01 except for one pair of designs (stiff 2 design and moderate 1 design) which was found to be statistically not very different as the significance level was higher than 0.01.

Furthermore, we performed the same experiments for stiff and flexible 1-BP-inserted structures (Supplementary Figures S9, S10, S12, S13, and Supplementary Tables S15–S18). Results for 6HB structures with 1-BP-insertion, however, showed an indistinguishable difference between the stiff (293 ± 16°) and flexible (291 ± 14°) designs (Supplementary Table S16). The trans ratios of stiff and flexible designs were not statistically different as the significance probability was 0.47. This might be because measuring a small difference in the twist angle for these 1-BP-inserted structures was hindered by the thermal fluctuation. Considering that the difference in the twist angle between the stiff and

flexible structures with 2-BP-insertion was 35.4° on average (Supplementary Table S16), the twist angle difference of 1-BP-inserted structures is expected to be approximately half of that (∼17.7°) assuming that the twist angle is proportional to the number of BP-insertion (Supplementary Note S2) supported by CanDo prediction (Supplementary Figure S10). However, the standard deviations of the twist angle for 1-BP-inserted structures were measured in the range of 13.8–16.0° (Supplementary Table S16) which amounts almost to the expected angle difference. Hence, it would be difficult to experimentally observe a significant difference in the 1-BP-inserted structures. Exceptional case in the 2-BP-inserted structures can be explained similarly. We, therefore, expect the proposed method for the twist control through the sequence design of nicks would be more effective for the design of highly twisted structures.

DISCUSSION

In summary, we quantified the sequence-dependent mechanical properties of DNA nicks using MD simulation. We found that nicks mainly exerted a softening effect in torsion, and their strength was dependent on the type and order of neighboring sequence. We applied this sequence-dependent effect to DNA origami design under mechanical analysis and proved the feasibility of finely controlling the twisted shape of DNA nanostructures by programming the sequences at nick sites experimentally.

Sequence design of nicks based on the C/B ratio was shown to be effective for twist control, but further studies would be necessary to verify the existence of more relevant and effective parameters by considering, for example, the anisotropic bending rigidities in our mechanical model. In future studies, when combined with existing coarse-grained computational modeling methods (9,16,17), our investigation of the mechanical properties of DNA nicks will be useful to enhance the accuracy and feasibility in designs ranging from sequence-level structures to super-structures beyond monomers. In addition, a kinetic measurement using reconfigurable DNA structures (20) would be beneficial to further investigate the sequence-dependent nick properties. The studies of DNA under constraints or external forces would also provide further insights into the effect of a nick on the mechanical properties and be useful in designing dynamic DNA nanostructures driven by external stimuli.

SUPPLEMENTARY DATA

Supplementary Data are available at NAR Online.

FUNDING

National Research Foundation of Korea [NRF-2017M3D1A1039422, NRF-2016R1C1B2011098]; National Institute of Supercomputing and Network/Korea Institute of Science and Technology Information with supercomputing resources including technical support [KSC-2018-S1-0013]. Funding for open access charge: National Research Foundation of Korea [NRF-2017M3D1A1039422].

Conflict of interest statement. None declared.

REFERENCES

1. Rothemund,P.W.K. (2006) Folding DNA to create nanoscale shapes and patterns. *Nature*, **440**, 297–302.
2. Dietz,H., Douglas,S.M. and Shih,W.M. (2009) Folding DNA into twisted and curved nanoscale shapes. *Science*, **325**, 725–730.
3. Chen,H., Zhang,H., Pan,J., Cha,T.G., Li,S., Andreasson,J. and Choi,J.H. (2016) Dynamic and progressive control of DNA origami conformation by modulating DNA helicity with chemical adducts. *ACS Nano*, **10**, 4989–4996.
4. Yoo,J. and Aksimentiev,A. (2013) In situ structure and dynamics of DNA origami determined through molecular dynamics simulations. *Proc. Natl. Acad. Sci. U.S.A.*, **110**, 20099–20104.
5. Maffeo,C., Yoo,J. and Aksimentiev,A. (2016) De novo reconstruction of DNA origami structures through atomistic molecular dynamics simulation. *Nucleic Acids Res.*, **44**, 3013–3019.
6. Lee,C., Lee,J.Y. and Kim,D.N. (2017) Polymorphic design of DNA origami structures through mechanical control of modular components. *Nat. Commun.*, **8**, 2067.
7. Goodman,R.P., Heilemann,M., Doose,S., Erben,C.M., Kapanidis,A.N. and Turberfield,A.J. (2008) Reconfigurable, braced, three-dimensional DNA nanostructures. *Nat. Nanotechnol.*, **3**, 93–96.
8. Song,J., Li,Z., Wang,P., Meyer,T., Mao,C. and Ke,Y. (2017) Reconfiguration of DNA molecular arrays driven by information relay. *Science*, **357**, eaan3377.
9. Kim,D.N., Kilchherr,F., Dietz,H. and Bathe,M. (2012) Quantitative prediction of 3D solution shape and flexibility of nucleic acid nanostructures. *Nucleic Acids Res.*, **40**, 2862–2868.
10. Veneziano,R., Ratanalert,S., Zhang,K., Zhang,F., Yan,H., Chiu,W. and Bathe,M. (2016) Designer nanoscale DNA assemblies programmed from the top down. *Science*, **352**, 1534.
11. Martin,T.G. and Dietz,H. (2012) Magnesium-free self-assembly of multi-layer DNA objects. *Nat. Commun.*, **3**, 2095.
12. Greene,D.G., Keum,J.W. and Bermudez,H. (2012) The role of defects on the assembly and stability of DNA nanostructures. *Small*, **8**, 1320–1325.
13. Ke,Y., Bellot,G., Voigt,N.V., Fradkov,E. and Shih,W.M. (2012) Two design strategies for enhancement of multilayer-DNA-origami folding: Underwinding for specific intercalator rescue and staple-break positioning. *Chem. Sci.*, **3**, 2587–2597.
14. Ma,Z., Huang,Y., Park,S., Kawai,K., Kim,D.N., Hirai,Y., Tsuchiya,T., Yamada,H. and Tabata,O. (2018) Rhombic-Shaped nanostructures and mechanical properties of 2D DNA origami constructed with different Crossover/Nick designs. *Small*, **14**, 1702028.
15. Praetorius,F., Kick,B., Behler,K.L., Honemann,M.N., Weuster-Botz,D. and Dietz,H. (2017) Biotechnological mass production of DNA origami. *Nature*, **552**, 84–87.
16. Pan,K., Kim,D.N., Zhang,F., Adendorff,M.R., Yan,H. and Bathe,M. (2014) Lattice-free prediction of three-dimensional structure of programmed DNA assemblies. *Nat. Commun.*, **5**, 5578.
17. Pan,K., Bricker,W.P., Ratanalert,S. and Bathe,M. (2017) Structure and conformational dynamics of scaffolded DNA origami nanoparticles. *Nucleic Acids Res.*, **45**, 6284–6298.
18. Kauert,D.J., Kurth,T., Liedl,T. and Seidel,R. (2011) Direct mechanical measurements reveal the material properties of three-dimensional DNA origami. *Nano Lett.*, **11**, 5558–5563.
19. O'Neill,P., Rothemund,P.W.K., Kumar,A. and Fygenson,D.K. (2006) Sturdier DNA nanotubes via ligation. *Nano Lett.*, **6**, 1379–1383.
20. Chen,H., Weng,T.W., Riccitelli,M.M., Cui,Y., Irudayaraj,J. and Choi,J.H. (2014) Understanding the mechanical properties of DNA origami tiles and controlling the kinetics of their folding and unfolding reconfiguration. *J. Am. Chem. Soc.*, **136**, 6995–7005.
21. Gore,J., Bryant,Z., Nollmann,M., Le,M.U., Cozzarelli,N.R. and Bustamante,C. (2006) DNA overwinds when stretched. *Nature*, **442**, 836–839.
22. Gross,P., Laurens,N., Oddershede,L.B., Bockelmann,U., Peterman,E.J.G. and Wuite,G.J.L. (2011) Quantifying how DNA stretches, melts and changes twist under tension. *Nat. Phys.*, **7**, 731–736.
23. Smith,S.B., Cui,Y. and Bustamante,C. (1996) Overstretching B-DNA: the elastic response of individual double-stranded and single-stranded DNA molecules. *Science*, **271**, 795–799.

24. Strick,T.R., Allemand,J.F., Bensimon,D., Bensimon,A. and Croquette,V. (1996) The elasticity of a single supercoiled DNA molecule. *Science*, **271**, 1835–1837.
25. Wang,M.D., Yin,H., Landick,R., Gelles,J. and Block,S.M. (1997) Stretching DNA with optical tweezers. *Biophys. J.*, **72**, 1335–1346.
26. Baumann,C.G., Smith,S.B., Bloomfield,V.A. and Bustamante,C. (1997) Ionic effects on the elasticity of single DNA molecules. *Proc. Natl. Acad. Sci. U.S.A.*, **94**, 6185–6190.
27. Moroz,J.D. and Nelson,P. (1997) Torsional directed walks, entropic elasticity, and DNA twist stiffness. *Proc. Natl. Acad. Sci. U.S.A.*, **94**, 14418–14422.
28. Bustamante,C., Smith,S.B., Liphardt,J. and Smith,D. (2000) Single-molecule studies of DNA mechanics. *Curr. Opin. Struct. Biol.*, **10**, 279–285.
29. Bryant,Z., Stone,M.D., Gore,J., Smith,S.B., Cozzarelli,N.R. and Bustamante,C. (2003) Structural transitions and elasticity from torque measurements on DNA. *Nature*, **424**, 338–341.
30. Lipfert,J., Kerssemakers,J.W., Jager,T. and Dekker,N.H. (2010) Magnetic torque tweezers: measuring torsional stiffness in DNA and RecA-DNA filaments. *Nat. Methods*, **7**, 977–980.
31. Lipfert,J., Wiggin,M., Kerssemakers,J.W., Pedaci,F. and Dekker,N.H. (2011) Freely orbiting magnetic tweezers to directly monitor changes in the twist of nucleic acids. *Nat. Commun.*, **2**, 439.
32. Herrero-Galán,E., Fuentes-Perez,M.E., Carrasco,C., Valpuesta,J.M., Carrascosa,J.L., Moreno-Herrero,F. and Arias-Gonzalez,J.R. (2012) Mechanical identities of RNA and DNA double helices unveiled at the single-molecule level. *J. Am. Chem. Soc.*, **135**, 122–131.
33. Olson,W.K., Gorin,A.A., Lu,X.J., Hock,L.M. and Zhurkin,V.B. (1998) DNA sequence-dependent deformability deduced from protein-DNA crystal complexes. *Proc. Natl. Acad. Sci. U.S.A.*, **95**, 11163–11168.
34. Lankas,F., Sponer,J., Hobza,P. and Langowski,J. (2000) Sequence-dependent elastic properties of DNA. *J. Mol. Biol.*, **299**, 695–709.
35. Kannan,S., Kohlhoff,K. and Zacharias,M. (2006) B-DNA under stress: over- and untwisting of DNA during molecular dynamics simulations. *Biophys. J.*, **91**, 2956–2965.
36. Fujii,S., Kono,H., Takenaka,S., Go,N. and Sarai,A. (2007) Sequence-dependent DNA deformability studied using molecular dynamics simulations. *Nucleic Acids Res.*, **35**, 6063–6074.
37. Lankas,F., Sponer,J., Langowski,J. and Cheatham,T.E. (2003) DNA basepair step deformability inferred from molecular dynamics simulations. *Biophys. J.*, **85**, 2872–2883.
38. Pasi,M., Maddocks,J.H., Beveridge,D., Bishop,T.C., Case,D.A., Cheatham,T., Dans,P.D., Jayaram,B., Lankas,F., Laughton,C. *et al.* (2014) μABC: a systematic microsecond molecular dynamics study of tetranucleotide sequence effects in B-DNA. *Nucleic Acids Res.*, **42**, 12272–12283.
39. Lavery,R., Zakrzewska,K., Beveridge,D., Bishop,T.C., Case,D.A., Cheatham,T., Dixit,S., Jayaram,B., Lankas,F., Laughton,C. *et al.* (2010) A systematic molecular dynamics study of nearest-neighbor effects on base pair and base pair step conformations and fluctuations in B-DNA. *Nucleic Acids Res.*, **38**, 299–313.
40. Perez,A., Lankas,F., Luque,F.J. and Orozco,M. (2008) Towards a molecular dynamics consensus view of B-DNA flexibility. *Nucleic Acids Res.*, **36**, 2379–2394.
41. Noy,A., Perez,A., Lankas,F., Luque,F.J. and Orozco,M. (2004) Relative flexibility of DNA and RNA: A molecular dynamics study. *J. Mol. Biol.*, **343**, 627–638.
42. Marin-Gonzalez,A., Vilhena,J.G., Perez,R. and Moreno-Herrero,F. (2017) Understanding the mechanical response of double-stranded DNA and RNA under constant stretching forces using all-atom molecular dynamics. *Proc. Natl. Acad. Sci. U.S.A.*, **114**, 7049–7054.
43. Liebl,K., Drsata,T., Lankas,F., Lipfert,J. and Zacharias,M. (2015) Explaining the striking difference in twist-stretch coupling between DNA and RNA: A comparative molecular dynamics analysis. *Nucleic Acids Res.*, **43**, 10143–10156.
44. Ma,N. and van der Vaart,A. (2016) Anisotropy of B-DNA groove bending. *J. Am. Chem. Soc.*, **138**, 9951–9958.
45. Leger,J.F., Romano,G., Sarkar,A., Robert,J., Bourdieu,L., Chatenay,D. and Marko,J.F. (1999) Structural transitions of a twisted and stretched DNA molecule. *Phys. Rev. Lett.*, **83**, 1066–1069.
46. Hase,F. and Zacharias,M. (2016) Free energy analysis and mechanism of base pair stacking in nicked DNA. *Nucleic Acids Res.*, **44**, 7100–7108.
47. Protozanova,E., Yakovchuk,P. and Frank-Kamenetskii,M.D. (2004) Stacked–unstacked equilibrium at the nick site of DNA. *J. Mol. Biol.*, **342**, 775–785.
48. Yakovchuk,P., Protozanova,E. and Frank-Kamenetskii,M.D. (2006) Base-stacking and base-pairing contributions into thermal stability of the DNA double helix. *Nucleic Acids Res.*, **34**, 564–574.
49. Lu,X.J. and Olson,W.K. (2003) 3DNA: a software package for the analysis, rebuilding and visualization of three-dimensional nucleic acid structures. *Nucleic Acids Res.*, **31**, 5108–5121.
50. Phillips,J.C., Braun,R., Wang,W., Gumbart,J., Tajkhorshid,E., Villa,E., Chipot,C., Skeel,R.D., Kale,L. and Schulten,K. (2005) Scalable molecular dynamics with NAMD. *J. Comput. Chem.*, **26**, 1781–1802.
51. Hart,K., Foloppe,N., Baker,C.M., Denning,E.J., Nilsson,L. and Mackerell,A.D. (2012) Optimization of the CHARMM additive force field for DNA: Improved treatment of the BI/BII conformational equilibrium. *J. Chem. Theory Comput.*, **8**, 348–362.
52. Jorgensen,W.L., Chandrasekhar,J., Madura,J.D., Impey,R.W. and Klein,M.L. (1983) Comparison of simple potential functions for simulating liquid water. *J. Chem. Phys.*, **79**, 926–935.
53. Essmann,U., Perera,L., Berkowitz,M.L., Darden,T., Lee,H. and Pedersen,L.G. (1995) A smooth particle mesh ewald method. *J. Chem. Phys.*, **103**, 8577–8593.
54. Feller,S.E., Zhang,Y.H., Pastor,R.W. and Brooks,B.R. (1995) Constant pressure molecular dynamics Simulation: The langevin piston method. *J. Chem. Phys.*, **103**, 4613–4621.
55. Brooks,B.R., Janežič,D. and Karplus,M. (1995) Harmonic analysis of large systems. I. Methodology. *J. Comput. Chem.*, **16**, 1522–1542.
56. Ivani,I., Dans,P.D., Noy,A., Perez,A., Faustino,I., Hospital,A., Walther,J., Andrio,P., Goni,R., Balaceanu,A. *et al.* (2016) Parmbsc1: a refined force field for DNA simulations. *Nat. Methods*, **13**, 55–58.
57. Douglas,S.M., Marblestone,A.H., Teerapittayanon,S., Vazquez,A., Church,G.M. and Shih,W.M. (2009) Rapid prototyping of 3D DNA-origami shapes with caDNAno. *Nucleic Acids Res.*, **37**, 5001–5006.
58. Norberg,J. and Nilsson,L. (1995) Stacking free-energy profiles for all 16 natural ribodinucleoside monophosphates in aqueous-solution. *J. Am. Chem. Soc.*, **117**, 10832–10840.
59. Brown,R.F., Andrews,C.T. and Elcock,A.H. (2015) Stacking free energies of All DNA and RNA nucleoside pairs and Dinucleoside-Monophosphates computed using recently revised AMBER parameters and compared with experiment. *J. Chem. Theory Comput.*, **11**, 2315–2328.
60. Hunter,C.A. and Lu,X.J. (1997) DNA base-stacking interactions: a comparison of theoretical calculations with oligonucleotide X-ray crystal structures. *J. Mol. Biol.*, **265**, 603–619.
61. Packer,M.J. and Hunter,C.A. (1998) Sequence-dependent DNA structure: the role of the sugar-phosphate backbone. *J. Mol. Biol.*, **280**, 407–420.
62. Kim,Y.J. and Kim,D.N. (2016) Structural basis for elastic mechanical properties of the DNA double helix. *PLoS One*, **11**, e0153228.